On the robustness of the r-process in neutron-star mergers against variations of nuclear masses

J J Mendoza-Temis[1,2], M R Wu[3], G Martínez-Pinedo[3,4], K Langanke[3,4], A Bauswein[5,6], H-T Janka[7] and A Frank[1,2]

[1]Instituto de Ciencias Nucleares, Universidad Nacional Autónoma de México, 04510 México, D.F., México
[2]Centro de Ciencias de la Complejidad, Universidad Nacional Autónoma de México, 04510 México, D.F., México
[3]Institut für Kernphysik (Theoriezentrum), Technische Universität Darmstadt, Schlossgartenstraße 2, 64289 Darmstadt, Germany
[4]GSI Helmholtzzentrum für Schwerionenforschung, Planckstraße 1, 64291 Darmstadt, Germany
[6]Heidelberger Institut für Theoretische Studien, Schloss-Wolfsbrunnenweg 35, 69118 Heidelberg, Germany
[5]Department of Physics, Aristotle University of Thessaloniki, 54124 Thessaloniki, Greece
[7]Max-Planck-Institut für Astrophysik, Postfach 1317, 85741 Garching, Germany

E-mail: `joel.mendoza@correo.nucleares.unam.mx`

Abstract. r-process calculations have been performed for matter ejected dynamically in neutron star mergers (NSM), such calculations are based on a complete set of trajectories from a three-dimensional relativistic smoothed particle hydrodynamic (SPH) simulation. Our calculations consider an extended nuclear reaction network, including spontaneous, β- and neutron-induced fission and adopting fission yield distributions from the ABLA code. In this contribution we have studied the sensitivity of the r-process abundances to nuclear masses by using diferent mass models for the calculation of neutron capture cross sections via the statistical model. Most of the trajectories, corresponding to 90% of the ejected mass, follow a relatively slow expansion allowing for all neutrons to be captured. The resulting abundances are very similar to each other and reproduce the general features of the observed r-process abundance (the second and third peaks, the rare-earth peak and the lead peak) for all mass models as they are mainly determined by the fission yields. We find distinct differences in the predictions of the mass models at and just above the third peak, which can be traced back to different predictions of neutron separation energies for r-process nuclei around neutron number $N = 130$.

1. Introduction

The astrophysical r process produces about half of the heavy elements in the Universe, including all of the actinides [1, 2]. It is commonly accepted that it occurs as a sequence of neutron captures and β decays in environments with extreme neutron densities. The natural candidate involves NSM, in fact numerical simulations indicate that the matter ejected during the dynamical phase is very neutron rich with extremely large neutron-to-seed ratios ($R_{n/s} > 400$) [3, 4, 5]; i.e. there are many neutrons which can be captured by seed nuclei transporting matter to very heavy nuclei in the region of the nuclear chart where decay by fission is possible. In this study, we work under the assumption that all ejecta remain neutron rich.

Nuclear masses are particularly important as they, via the neutron separation energies, define the r-process path in the nuclear chart and secondly they are crucial ingredients in the statistical model calculation of neutron capture cross sections. As the masses of the extremely neutron-rich nuclei on the r-process path are not known experimentally, they have to be modeled. We use four different mass models (FRDM [6], HFB21 [7], WS3 [8] and DZ31 [9, 10]) for the calculation of the neutron capture rates that enter in the r-process simulations. Despite there are two recent sensitivity studies already available, on the one hand randomly varying individual masses [11], and on the other hand exploring systematic uncertainties for masses estimated via different energy density functionals [12]; in this contribution we aim at determining the nuclear origin of the robust r-process pattern observed in several NSM simulations. It is often stated that NSM produce a robust r-process due to fission cycling. However, this statement simply expresses the fact that fission cycling is unavoidable due to the large neutron-to-seed ratios ($R_{n/s}$) reached in NSM ejecta without really explaining the nuclear mechanism responsible for the robustness. Our paper is organized as follows. In the next section we give a brief description of our r-process simulations and the input being used. The results of our simulations for the r-process abundances and their dependence on the adopted mass models are presented and discussed in section 3. Finally, we conclude in section 4.

2. NSM trajectories and nuclear input

We have calculated the r-process abundances for 528 trajectories with a total ejected mass of $\sim 1.70 \times 10^{-3}$ $M_\odot$ comming from a binary system of two NSs with gravitational masses of 1.35 $M_\odot$, which may be representative for the observed double NS systems (see e.g. [13] for a compilation of measured binary NS masses). In a previous work [14] such trajectories were classified with respect to two competing rates: the depletion rate due to neutron captures on seed nuclei (λ_n) and the hydrodynamic expansion rate (λ_d). "Slow ejecta" corresponds to most of the trajectories (484 trajectories with a total mass of $\sim 1.57 \times 10^{-3}$ $M_\odot$), where nearly all initial neutrons can be captured as $\lambda_n \gtrsim \lambda_d$ until the end of the r process at ~ 1 s. On the other hand, about $\sim 10\%$ of the ejecta (44 trajectories, $\sim 1.28 \times 10^{-4}$ $M_\odot$) initially expand extremely fast ("fast ejecta"), and as a consequence free neutrons are left at the end of the r process. We have started our r-process calculations at temperatures of $T = 6$ GK, with densities ranging from $\rho \sim 10^7$ g cm^{-3} to $\sim 3 \times 10^{13}$ g cm^{-3}. The initial matter compositions have been determined assuming the matter to be in Nuclear Statistical Equilibrium (NSE). The initial neutron-to-seed ratios ($R_{n/s}$) of those ejecta range from 400 to 2000. Starting from these initial compositions we have followed the r-process evolution by a large network including more than 7300 nuclei which cover the nuclear chart from free nucleons up to ^{313}Ds. The dynamics of the r-process was governed by the astrophysical trajectories, however, consistently corrected for reheating by energy release in nuclear reactions (for more details see [14]). As nuclear reactions among these nuclei we considered charge particle reactions, neutron captures and its inverse process, photo-dissociation, and β and α decay and fission. We have derived the neutron capture rates consistently for each individual mass model within the statistical model using the code MOD-Smoker [15]. The photodissociation rates were obtained from the neutron capture rates by detailed balance. For nuclei, for which the half lives are not known experimentally, we have adopted the β decay (and β delayed neutron emission) rates from the compilation of Möller *et al.* [16], which was derived from QRPA calculations on top of the FRDM mass model. We used the parametrization of Ref. [17] of the Viola-Seaborg formula to estimate the α-decay rates, which become relevant for heavy nuclei beyond lead. Finally, for nuclei with $Z > 83$, where a competition between (n, γ) and neutron induced fission can take place, we used neutron-induced reaction rates taken from [18] that are based on the FRDM mass model [6] and the Thomas-Fermi fission barriers of Myers and Swiatecki [19]. Rates for β delayed and spontaneous fission were adopted from [20]. Our fission yields were taken from the calculations of Ref. [21] which

were derived using the code ABLA. This approach also gives a consistent estimate for the number of neutrons set free during the fission process.

3. Results

3.1. Evolution of the r-process abundances for the slow ejecta

For the r-process nucleosynthesis of the so-called slow ejecta we show in Fig. 1, the abundances at 3 different phases of the evolution: a) at freeze out, which we define as the moment where $R_{n/s} = 1$, b) the moment when the average timescale for β decays becomes equal to the average timescale for neutron captures, c) the final abundance, calculated at a time of 1 Gyr.

At freeze-out, the abundances show a strong odd-even staggering, moreover nuclei are pushed into the transuranium region, where the nuclei with largest abundances are located around $A \sim 280$ corresponding to the $N = 184$ shell closure, such nuclei have lower barriers and consecuently n-induced fission dominates over n-capture, and the r-process cycles to medium mass nuclei rather than producing heavier nuclei. In addition fission is also an important source of free neutrons, under such conditions the total number of neutrons produced can be divided into two components: 1) a prompt component that consists of the neutrons evaporated mainly by the highly excited fragments, and 2) a delayed component that occurs during the decay of the fragments to the instantaneous r-process path.

Once neutron captures are slower than β decays, matter decays to stability. In particular, the significant amount of matter above lead, still existing in the middle panels of figure 1, decays to finally form the lead peak. At 1 Gyr only the long-lived thorium and uranium isotopes survive. When comparing the time evolution of the third peak (from the upper to the middle to the lower panel of figure 1) one clearly notices a shift of the third peak to slightly larger mass numbers in the FRDM and HFB21 mass model but absent in the WS3 and DZ31 mass models. To understand the reason for this behavior it is important to remember that the r process operates along a path of almost constant neutron separation energy. The speed at which the r process proceeds from lighter nuclei to heavier nuclei depends on the beta-decay half-lives which increase with increasing mass number. On top of this global behavior, there are local effects induced by the presence of neutron shell closures. In the r-process path nuclei with $N \gtrsim 82$ and $N \gtrsim 126$ have the longest half-lives. At freeze-out, it corresponds to charge numbers $Z \approx 48$ and $Z \approx 70$, respectively. Alternatively, the effective r-process timescale in the region can change if the r-process path changes due to modifications of the underlying mass model. Different mass models differ substantially in their predictions in regions where there is a sudden change in the intrinsic deformation [22]. This is particularly the case around $N \sim 90$ and $N \sim 130$ where all mass models used in the present work predict a transition from spherical to deformed configurations. The particular relevance for the r process is the fact that this transition can be associated with a sudden drop in the neutron separations energies. This is the case for the FRDM mass model and its most noticeable consequence is the presence of a narrow peak around $A \sim 136$ at freeze-out (see upper panel for FRDM mass model in Fig. 1). Due to the accumulation of material in this region, the r process lasts slightly longer using the FRDM mass model when compared with the other models. The peak becomes washed out at later times due to continuous production of material in this region by fission. However, neutron captures on the fission yields are responsible for a flow of matter from the second r-process peak to heavier nuclei. This flow operates in all used mass models except in FRDM due to the fact that material is halted at $N \sim 90$.

The third peak abundance is noticeably more sensitive to nuclear masses that influence the neutron capture rates. For two of the mass models (FRDM, HFB21) the peak width is noticeably narrower than observed, the peak height is overestimated, the position shifted slightly to larger mass numbers and an abundance trough is predicted just above the peak as can be seen in Fig. 1. This is because the FRDM and HFB21 mass models predict noticeably smaller neutron separation energies than the Duflo-Zuker or the WS3 models at $N = 130$, just above the magic

number $N = 126$. Thus these nuclei act as (additional) obstacles in r-process simulations. In summary, the third peak in the abundance distribution shift to higher mass numbers is caused mainly by late-time neutron captures.

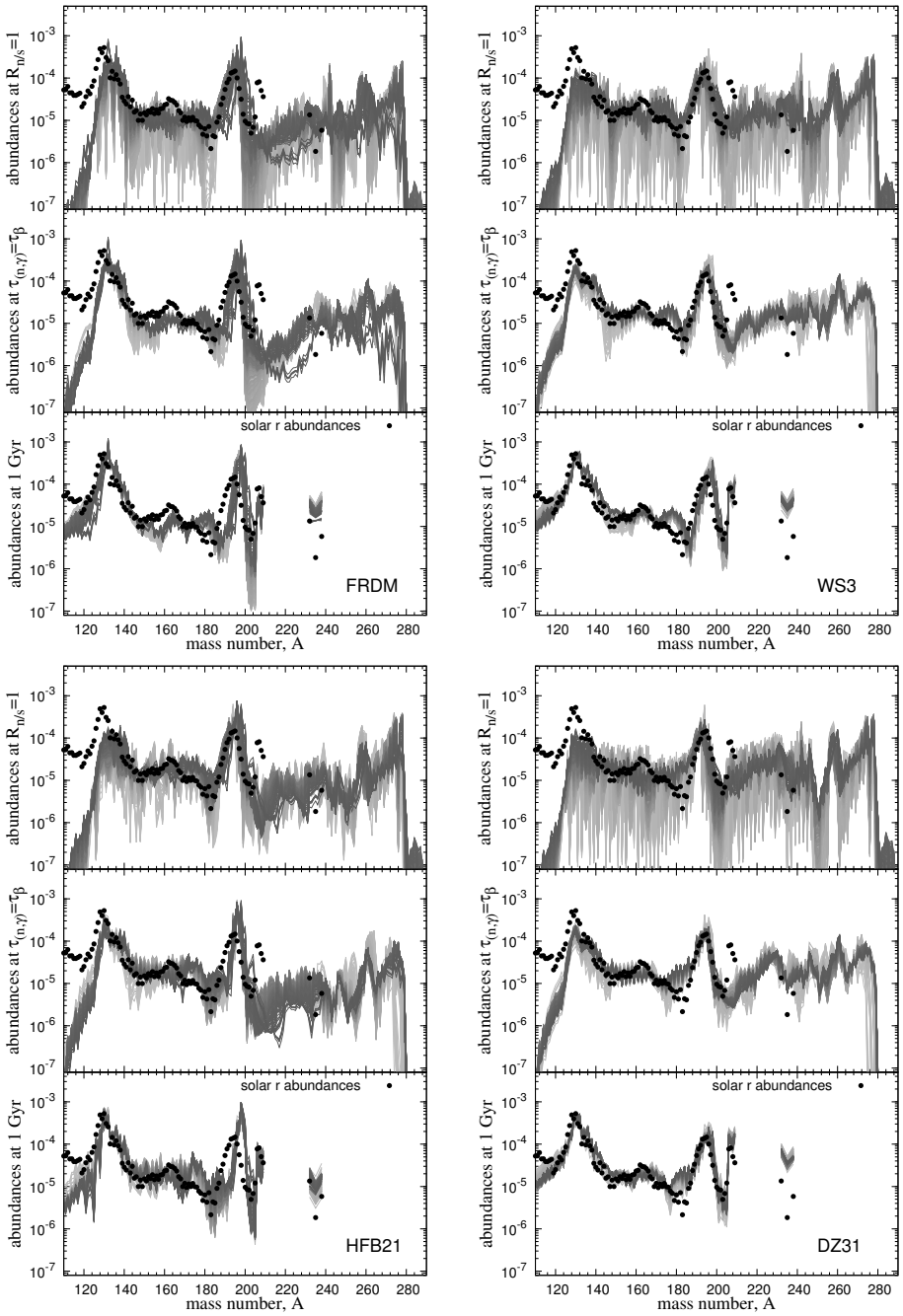

Figure 1. (Color online) R-process abundances of the slow ejecta for different mass models at different phases of the evolution. The upper panels show the abundances at $R_{n/s} = 1$. The middle panel at the time where the average timescales for beta-decay and neutron captures become identical. The lower panel shows the abundances at 1 Gyr when most of the material has already decayed to the stability.

3.2. Evolution of the r-process abundances for fast ejecta

In Fig. 2 we show r-process abundances obtained for the fast ejecta at three different phases of the evolution and for the 4 different mass models. The top panel, for each mass model, shows the abundances before the "last" fission cycle, when the average mass number $\langle A \rangle$ reaches the final maximum. The middle panel exhibits the freeze-out abundances at $\tau_{(n,\gamma)} = \tau_\beta$ rather than by $R_{n/s} = 1$, and the lower panel shows the final r-process abundances at 1 Gyr.

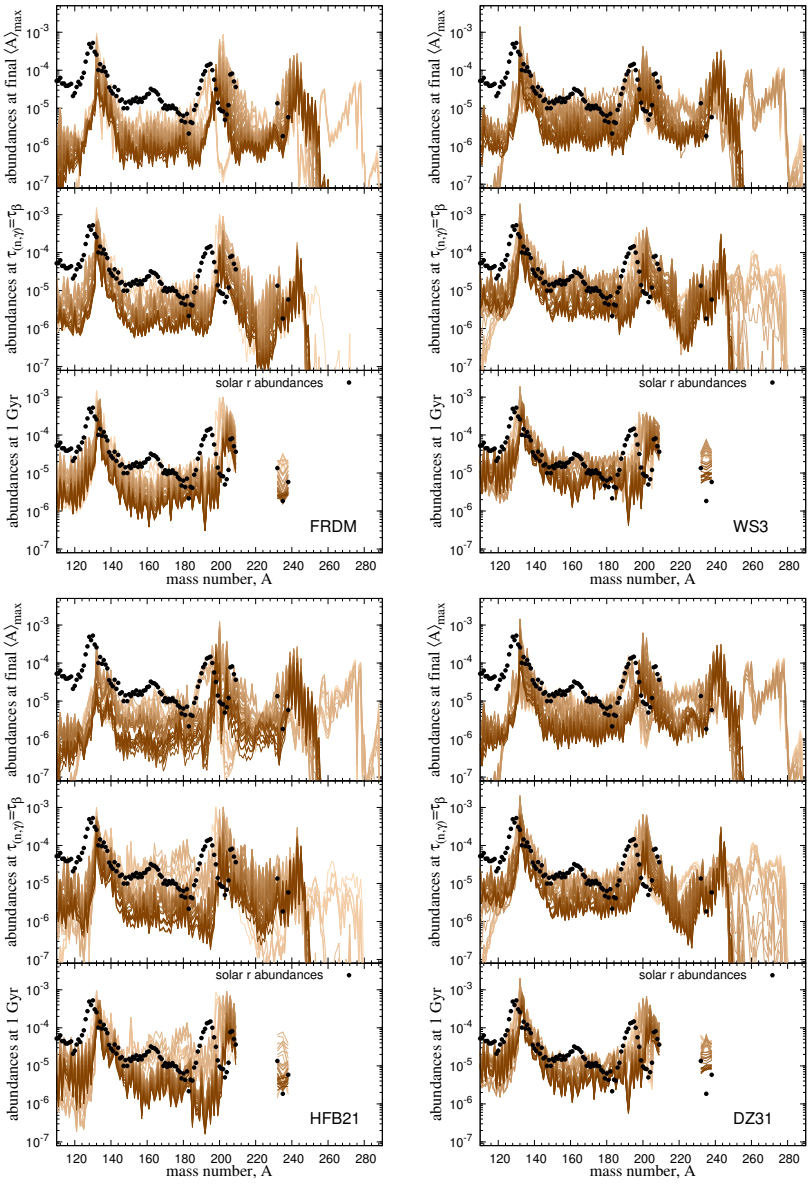

Figure 2. (Color online) R-process abundances of fast ejecta for different mass models at different phases of the evolution. The upper panels show the abundances at times before the "last" fission cycle, when the average mass number $\langle A \rangle$ reaches the final maximum. The middle panel at the time where the average timescales for beta-decay and neutron captures become identical. The lower panel shows the abundances at 1 Gyr when most of the material has already decayed to the stability.

Due to the slower neutron capture rates, the r-process path for the fast ejecta runs noticeably closer to the region of stability. This has several consequences: First, the position of third r-process peak, related to nuclei with magic neutron number $N = 126$, is shifted to larger mass numbers around $A \sim 200$. Second, under the conditions of fast expansion, and slow neutron captures, the nuclei with magic neutron numbers $N = 82$ are a noticeable obstacle for the mass flow towards heavier nuclei. Third, neutron captures are too inefficient to replenish the region of $A \sim 280$ prior to the last fission cycle for most of the trajectories. As a consequence, the subsequent decay of these heavy nuclei by fission contributes only rather modestly to the r-process abundances around the second peak at $A \sim 130$, as can be seen in the lower panels of Fig. 2. However, the decay of matter beyond the third peak, after freeze-out, fills up the abundances around lead.

In contrast to the slow ejecta, the fast ejecta exhibit a large spread in the final abundances observed between the different trajectories. This points to a very strong sensitivity to details of the astrophysical conditions and to the nuclear properties, if neutron captures are slow during the r process. In fact, the fast ejecta, encountered in our NSM scenario, resemble a nucleosynthesis process somewhat between r-process and s-process.

3.3. Robust r-process abundances

Fig. 3 shows the final abundances at times of 1 Gyr for all individual NSM trajectories and for all the mass models. Additionally, the figure exhibits mass-averaged abundances for all trajectories (red curves), for the slow trajectories (green curves), and for the fast ejecta (blue curves), respectively. To better visualize the contribution of slow and fast ejecta to the total ejected mass we have multiplied the slow and fast trajectories and their averages by the fractional contribution of each ejecta, i.e. ~ 0.9 for the slow and ~ 0.1 for the fast ejecta.

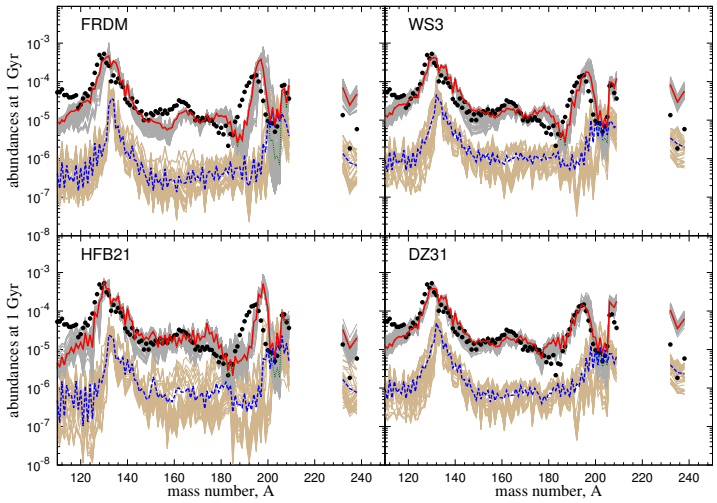

Figure 3. (Color online) Final r-process abundances at a time of 1 Gyr for the different mass models and all trajectories used in the calculations. The grey (brown) curves correspond to the abundances of the trajectories of the slow (fast) ejecta shown previously in the bottom panels of Fig. 1 and 2 but without the color gradient. The mass-averaged abundances for all trajectories (red curves), the slow ejecta (green curves), and the fast ejecta (blue curves) are also shown. The abundances for the slow and fast trajectories and their averages have been scaled by the value of their fractional contribution to the total ejecta.

As already stressed above, the most striking feature of our calculations is the fact that the final abundances for mass numbers $A > 120$ are virtually identical, for a given mass model, for all the slow ejecta, while they vary noticeably for the fast ejecta. Furthermore, the total mass-averaged abundances show the same pattern as those for the slow ejecta, as these constitute the dominating part of the ejected mass. We hence conclude that dynamical ejecta of NS mergers show a robust r-process pattern, as already concluded in refs. [3, 4, 5], provided that Y_e in the ejecta remains low, see refs [23, 24, 25]. We find that the main requirement to achieve a robust r-process pattern is that the amount of material accumulated at freeze-out in the fissioning region, $A \gtrsim 250$ is much larger than the one present in the region below the 3rd r-process peak. For the slow ejecta, this is guaranteed by the fact that the beta-decay half-lives grow with increasing mass number and by the presence of a neutron shell closure around $N = 184$. Both effects are responsible of producing a peak in the freeze-out r-process abundances around $A \sim 280$ (see upper panels Fig. 1). The material in this peak decays by fission contributing to the abundances around the 2nd r-process peak and producing a final robust r-process pattern. For the fast ejecta, the lack of material accumulated in the $A > 250$ region, due to the much slower neutron capture rates at later stage of the r-process, results in reduced impact of fission yields on the final distributions and in a much larger spread of the final abundance distributions. However, these trajectories contribute only mildly to the final mass-integrated abundances except for the region around $A = 200$.

The general features of this pattern is also independent of the mass models as it is mainly determined by fission yields. This is demonstrated in Fig. 4 where we compare the final mass-integrated abundances (at 1 Gyr) for four different mass models (FRDM, WS3, HFB21, DZ31). Although there are specific differences originating in the dependence of neutron captures on the underlying mass model, all the calculations reproduce the second and third r-process peaks reasonably well. We mention again that the peaks have different origins in our simulations: the peak around $A \sim 130$ arises from fission yields, while the peak at $A \sim 195$ reflects the $N = 126$ waiting points in the matter flow towards heavy nuclei. It is also satisfying to observe that the lead peak around $A \sim 208$ agrees reasonably well with the solar abundances. This peak is mainly produced by α decay of heavier nuclei. Finally also the abundances of the long-lived isotopes ^{232}Th and ^{238}U, which are the final product of some matter with charge numbers $Z \approx 90 - 96$, is reproduced reasonably well.

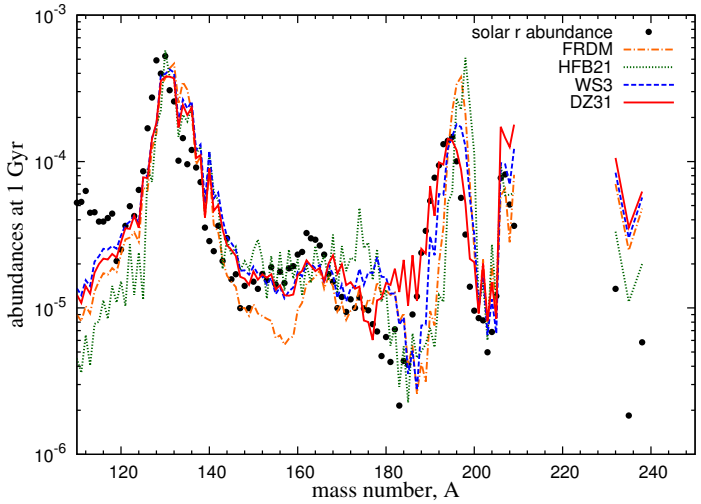

Figure 4. (Color online) Final mass-integrated abundances for all trajectories at a time of 1 Gyr for all mass models considered in this work.

4. Conclusions

We have been able to reproduce the main features of the r-process abundances (the second and third peaks, the rare-earth peak and the lead peak) reasonably well. There are modest differences in the position of the third peak and in abundance distribution just above this peak around $A \sim 205$. Here experimental work is needed to resolve these different mass predictions for the $N = 130$ nuclei.

Most of our simulations corresponding to 90% of the ejected mass, support the hypothesis that the r-process in dynamical ejecta from NSM yield rather robust abundance distribution in good agreement with the observed solar distribution for nuclei with $A \gtrsim 120$. We have shown that a requirement to achieve such a robust pattern is that at freeze-out the amount of material accumulated in the fissioning region ($A \gtrsim 250$) is much larger than the material located in the second r-process peak and above ($A \approx 120$–180). To achieve these astrophysical conditions, a sufficiently large neutron-to-seed ratio ($R_{n/s}$) is required, which, together with the fact that beta-decay half-lives along the r-process path grow with increasing mass number, guarantees the pile up of material in the fissioning region. The decay of this material by fission produces a robust r-process pattern in the region $A \approx 120$-180 that, however, depends on the used fission yields (see ref. [26]). This pattern is slightly modified by late neutron captures during the decay back to stability, which also introduces a small dependence on the astrophysical conditions.

Further extensions of the present work, need to address the impact of variations of nuclear masses for the calculation of fission and beta-decay rates.

Acknowledgments

J.J. Mendoza-Temis is a DGAPA-UNAM fellow and thanks to CONACYT project number 155663 for its support.

References

[1] Burbidge E M, Burbidge G R, Fowler W, and Hoyle F 1957 *Rev. Mod. Phys.* **29** 547
[2] Cameron A G W 1957 *Stellar Evolution, Nuclear Astrophysics, and Nucleogenesis*, Chalk River Report **CRL-41**
[3] Goriely S, Bauswein A, and Janka H T 2011 *Astrophys. J.* **738** L32
[4] Korobkin O, Rosswog S, Arcones A, and Winteler C 2012 *Mon. Not. R. Astron. Soc.* **426** 1940
[5] Bauswein A, Goriely S, and Janka H T 2013 *Astrophys. J.* **773** 78
[6] Möller P, Nix J R, Myers W D, and Swiatecki W J 1995 *At. Data Nucl. Data Tables* **59** 185
[7] Goriely S, Chamel N, and Pearson J M 2010 *Phys. Rev. C* **82** 035804
[8] Liu M, Wang N, Deng Y, and Wu X 2011 *Phys. Rev. C* **84** 014333
[9] Duflo J, and Zuker A P 1995 *Phys. Rev. C* **52** R23
[10] Mendoza-Temis J, Hirsch J G, and Zuker A P, Nuclear Physics A **843** (1), 14-36 (2010)
[11] Mumpower M, Surman R, McLaughlin G C, and Aprahamian A 2016 *Prog. Part. Nucl. Phys.* **86** 86
[12] Martin D, Arcones A, Nazarewicz W, and Olsen E 2016 *Phys. Rev. Lett.* **116** 121101
[13] Lattimer J M 2012 *Annu. Rev. Nucl. Part. Sci.* **62** 485
[14] Mendoza-Temis J J, Wu M R, Langanke K, Martínez-Pinedo G, Bauswein A, and Janka H T 2015 *Phys. Rev. C* **92** 055805
[15] Loens H P 2010 *Ph.D. thesis, TU Darmstadt* (unpublished)
[16] Mller P, Pfeiffer B, and Kratz K L 2003 *Phys. Rev. C* **67** 055802
[17] Dong T and Ren Z 2005 *Eur. Phys. J. A* **26** 69
[18] Panov I V, Korneev I Y, Rauscher T, Martínez-Pinedo G, Kelić-Heil A, Zinner N T, and Thielemann F K 2010 *Astron. Astrophys.* **513** A61
[19] Myers W D, and Swiatecki W J 1999 *Phys. Rev. C* **60** 014606
[20] Petermann I, Langanke K, Martínez-Pinedo G, Panov I V, Reinhard P G, and Thielemann F K 2012 *Eur. Phys. J. A* **48** 122
[21] Zinner N T 2007 *Ph.D. thesis, University of Aarhus* (unpublised)
[22] Arcones A and Martínez-Pinedo G 2011 *Phys. Rev. C* **83** 045809
[23] Wanajo S, Sekiguchi Y, Nishimura N, Kiuchi K, Kyutoku K, and Shibata M 2014 *Astrophys. J.* **789** L39
[24] Sekiguchi Y, Kiuchi K, Kyutoku K, and Shibata M 2015 *Phys. Rev. D* **91** 064059

[25] Goriely S, Bauswein A, Just O, Pllumbi E, and Janka H T 2015 *Mon. Not. R. Astron. Soc.* **452** 3894
[26] Goriely S, and Martínez-Pinedo G 2015 *Nucl. Phys. A* **944** 158.